Title

Microbial iron uptake as a mechanism for dispersing iron from deep-sea hydrothermal vents

Meng Li[1], Brandy M. Toner[4], Brett J. Baker[1], John A. Breier[5], Cody S. Sheik[1] and Gregory J. Dick[1,2,3*]

[1]Department of Earth and Environmental Sciences, [2]Department of Ecology and Evolutionary Biology, [3]Center of Computational Medicine and Bioinformatics, University of Michigan, Ann Arbor, MI 48109

[4]Department of Soil, Water, and Climate, University of Minnesota-Twin Cities, St. Paul, MN 55108

[5]Woods Hole Oceanographic Institution, Woods Hole, MA 02543, USA

*Correspondence: GJ Dick (gdick@umich.edu)

Department of Earth and Environmental Sciences, The University of Michigan, 2534 CC Little Building, 1100 North University Avenue, Ann Arbor MI, 48109-1005, USA.

Abstract

Deep-sea hydrothermal vents are a significant source of oceanic iron. Although hydrothermal iron rapidly precipitates as inorganic minerals upon mixing with seawater, it can be stabilized by organic matter and dispersed more widely than previously recognized. The nature and source of this organic matter is unknown. Here we show that microbial genes involved in cellular iron uptake are highly expressed in the Guaymas Basin deep-sea hydrothermal plume. The nature of these microbial iron transporters, taken together with the low concentration of dissolved iron and abundance of particulate iron in the plume, indicates that iron minerals are the target for this microbial scavenging and uptake. Our findings indicate that cellular iron uptake is a major process in plume microbial communities and suggest new mechanisms for generating Fe-C complexes. This "microbial iron pump" could represent an important mode of converting hydrothermal iron into bioavailable forms that can be dispersed through the oceans.

Introduction

Iron (Fe) is the fourth most abundant element in the Earth's crust but it is exceedingly rare in the oceans[1]. Fe-enrichment experiments show that Fe supply stimulates phytoplankton growth and hence the biological carbon pump, which sequesters carbon to the deep ocean[2]. Because it is such a limiting nutrient, marine microorganisms employ multiple strategies for obtaining Fe in various forms including dissolved Fe, particulate Fe (i.e. minerals), and Fe tightly bound to organic complexes like siderophores, hemophores, and heme[3]. Cells transport these Fe-organic complexes through specific membrane receptors, such as TonB-dependent

transporters and ATP binding cassette (ABC) transporters, for subsequent biological utilization or storage[4]. However, an excess of Fe is toxic because of its ability to form reactive oxygen species[4,5]. Therefore, microbial Fe uptake is tightly controlled to maintain desirable intracellular Fe concentrations, often by the enzyme ferric uptake regulator (Fur)[4,5]. Fe sequestered by bacteria in this way is responsible for a large portion of Fe acquisition by marine phytoplankton in surface oceans[6].

Mid-ocean ridge axial hydrothermal venting contributes an annual flux of 1000-10,000 Gg of dissolved Fe to the oceans[7]. It is commonly assumed that most of this Fe is biologically inaccessible due to the rapid chemical precipitation of Fe sulfide or oxide minerals[8]. However, recent evidence suggests that organic compounds bind and stabilize Fe in hydrothermal plumes, potentially altering the fate of Fe derived from hydrothermal vents[9-14]. Indeed, hydrothermal Fe may be transported thousands of kilometers from the source and represent a major source of Fe to deep ocean basins[13,15,16]. The nature and source of the organic ligands of Fe in plumes are unknown, but previous studies highlight the potential importance of microbial processes[9-11].

To investigate the mechanisms by which microorganisms influence cycling of hydrothermal Fe, we analyzed whole community gene expression (metatranscriptomics) together with Fe speciation (thermodynamic modeling and spectromicroscopy) of deep-sea hydrothermal plume (~1950 m) and background seawater (above the plume, ~1600 m) in the Guaymas Basin (GB), Gulf of California. We propose that the microbial uptake of iron from hydrothermal plume minerals represents a “microbial iron pump” in which inorganic iron is converted into more bioavailable and mobile forms that can be dispersed throughout the oceans.

Results

Microbial Fe uptake genes in plume metatranscriptomes. Shotgun sequencing of community RNA with the Illumina HiSeq-2000 platform produced 206 and 245 million short read transcript sequences from plume and background samples, respectively (Supplementary Table 1). We used a database of genes for cellular Fe uptake and utilization processes[17,18] to identify 28,338 transcripts of genes encoding various Fe acquisition pathways. Transcripts of Fe-related genes were more abundant in plume than background, and similar results were observed in data obtained from 454 sequencing technology (Supplementary Fig. 1). The enrichment of transcripts of Fe-related genes in the plume suggest that Fe acquisition is crucial for supporting the enhanced microbial growth that occurs via chemosynthesis in deep-sea hydrothermal plumes[19]. To facilitate further analysis of these Fe-related genes, metatranscriptomic reads were assembled *de novo*[20], yielding 154 different Fe uptake genes in the plume. Several of these Fe-related genes were among the most abundantly represented genes in the entire plume metatranscriptome, including genes encoding TonB-dependent receptors and ABC-type transporters (Fig. 1). Of the total Fe-related transcripts identified in the plume, nearly 77% are from just five categories, including siderophore synthesis and uptake, Fe(III) uptake, siderophore regulation, and unspecified Fe transport (Fig. 2). Genes for heme uptake, Fe(II) uptake, Fe storage and other biological functions were present but less abundant (Fig. 2).

Fe-related genes were further analyzed for their taxonomic affiliation using BLAST searches against the non-redundant NCBI protein database. *Gammaproteobacteria*, primarily *Alteromondaceae*, *Methylococcaceae* and uncultured SUP05, dominated Fe-related genes in the metatranscriptome, accounting for 26% to 87% of transcripts from the top five pathways (Fig. 3). The SAR324 group

of *Deltaproteobacteria* also has several highly expressed genes encoding putative Fe ABC transporters, which dominate the unspecified Fe transport pathway (Fig. 3). *Methylococcaceae*, uncultured SUP05, and SAR324 were identified previously as the major community members in the GB plume[21]. Despite the low abundance of *Alteromondaceae* in the Guaymas Basin (averaging 2.8 times coverage for metagenome and 1.01-4.04% of the total Guaymas Basin community at depths of 1300-1900 m)[20], their Fe uptake genes accounted for 12% to 45% of transcripts for the five dominant Fe uptake pathways (Fig. 3). Further analysis of the main *Alteromondaceae* group in the GB metatranscriptome (designated "GBAlt") indicated that it was closely related to the ubiquitous particle-associated marine heterotroph *Alteromonas macleodii*[22] (Supplementary Fig. 2, 3). Interestingly, GBAlt has highly transcribed genes encoding TonB-dependent and ABC transporters, including those predicted to be involved in transport of Fe-siderophores or Fe-heme/hemophores (Fig. 1, Supplementary Fig. 4). Taken together, these results show that many of the dominant bacterial groups of the GB hydrothermal plume participate in cellular Fe uptake, including methanotrophs (*Methylococcaceae*), chemolithoautotrophs (SUP05 and SAR324), and heterotrophs (*Alteromondaceae*).

More than 70% of the Fe-related transcripts we identified are involved in pathways for siderophore uptake, regulation and biosynthesis (Fig. 2), indicating that siderophores are a key mechanism for microbial Fe uptake in the GB hydrothermal plume community. Siderophores are low molecular weight organic ligands that bind Fe(III) with high affinity and specificity. Two predominant structural classes of marine siderophores have been identified: (a) amphiphilic siderophores with fatty acid appendages of various lengths, and (b) siderophores with α-hydroxy carboxylic acid moieties. The majority of siderophores identified to date are from

Gammaproteobacteria and *Alphaproteobacteria*[23]. Our results are consistent with *Gammaproteobacteria* being the dominant producers of siderophores in the GB plume, accounting for 66% of Fe transcripts putatively involved in siderophores synthesis (Fig. 3). Determining the molecular structure of siderophores in complex samples such as seawater is notoriously difficult[23-25]. The genes involved in siderophore biosynthesis, regulation, and uptake identified here may provide unique insights into the nature, source, and factors controlling the abundance of siderophores in plumes. However, accurate prediction of siderophore structures from genetic data is not currently feasible due to the dearth of biochemical and physiological data on the microbial groups described here, which are mostly uncultured. Siderophore production is widespread in *Alteromonas* species, and *Alteromonas macleodii* takes up siderophores but does not produce siderophores[26,27], suggesting that it may utilize exogenous siderophores or other natural organic ligands.

Physicochemical measurement and thermodynamic modeling. Our metatranscriptomic data indicate that plume microorganisms obtain Fe primarily in the form of Fe(III) rather than Fe(II). This finding is consistent with previous results from geochemical modeling, which show that Fe(III) rather than Fe(II) binding ligands are more efficient at stabilizing hydrothermal iron for transport away from the near vent field[11]. Previous work has also shown that total Fe concentrations in endmember GB hydrothermal fluids range from 1.7×10^{-5} to 18×10^{-5} mol/kg[28], orders of magnitude higher than in background seawater. Given this high abundance of Fe, the prevalence of Fe scavenging mechanisms is somewhat surprising. However, upon mixing of hydrothermal fluids with seawater, much of the soluble, readily bioavailable Fe(II) precipitates as oxides and sulfides that are less bioavailable. To

assess the speciation and concentration of Fe in the GB plume, we used thermodynamic modeling, X-ray absorption spectroscopy (XAS), scanning transmission X-ray microscopy (STXM) and elemental analysis by inductively coupled plasma optical emission spectroscopy. Modeling conducted in the absence of organic ligands predicts that aqueous phase Fe(II) and Fe(III) species are at low concentration (ca. < 0.1 nmol kg^{-1} seawater). Measured concentrations of particulate Fe ranged from 4.15-15.78 nmol kg^{-1} seawater (Supplementary Table 2). Elemental analyses also confirm the significant fraction of hydrothermal material in these samples, which exhibit Al/(Al+Fe+Mn) ratios of 0.4 to below our detection limit for Al[29]. Modeling results predict particulate Fe species including pyrite, magnetite, and Fe(III)-hydroxide (Fig. 4a, Supplementary Fig. 5). Consistent with model predictions, Fe(III)-bearing (oxyhydr)oxide minerals such as maghemite (γ-$Fe(III)_2O_3$), lepidocrocite (γ-Fe(III)OOH), and magnetite ($Fe(II)Fe(III)_2O_4$) were observed by Fe 1s X-ray absorption near edge structure (XANES) spectroscopy (Fig. 4b, 4c). STXM revealed that plume particles (4-10 µm diameter range) are composed of aggregated materials that are rich in Fe as well as carbon, nitrogen, and manganese (Supplementary Fig. 6, 7). The C 1s XANES spectra are consistent with primarily aliphatic organic molecules having C=C (285.2 eV), -CH (287.5 eV), and O-C=O (288.7 eV) functional moieties (Supplementary Fig. 8), distinct from the protein and lipid-rich particulate organic carbon (POC) observed in plumes at the East Pacific Rise[9,12].

Discussion

Given the prevalence of siderophore-mediated Fe(III) uptake in the GB plume microbial community and that plume Fe is expected to be predominant in the form of

particulate minerals, we propose a model for microbial acquisition of Fe through microbe-mineral interactions in hydrothermal plumes (Fig. 5). Under low dissolved Fe conditions and to support the growth that occurs in the presence of hydrothermal energy sources, microbes produce a variety of siderophores that dissolve solid phase Fe minerals and facilitate cellular uptake[30]. Siderophore production is regulated by ferric uptake regulator to maintain Fe homeostasis[3]. Fe(III) is reduced to Fe(II) within the cell for storage or use in biological functions in which it is complexed to a variety of intracellular organic compounds[4]. Subsequent cell death may release this organically complexed Fe into the dissolved or particulate organic carbon pool. Alternatively, because deep-sea microbial communities are thought to be relatively stable[19], Fe that remains within cells would be widely dispersed by deep ocean currents. In either case, these processes represent a "microbial Fe pump" that mobilizes Fe bound in minerals and sequesters it within organic material where it is protected from oxidation and scavenging. This is a distinct but not mutually exclusive mechanism for plume Fe-carbon interactions compared to others that have been put forward. For example, the microbial Fe pump could generate Fe bound to POC or dissolved organic carbon (DOC) that has been observed previously[9-11]. An important distinction, however, is that siderophore-mediated mobilization of Fe(III) from minerals greatly expands the region in which organic complexation could take place because previous mechanisms require complexation prior to or immediately after Fe(II) oxidation[10], and are thus tied to Fe(II) oxidation kinetics. In contrast, a siderophore-mediated mechanism could operate long after precipitation of Fe minerals as plumes disperse far from hydrothermal fields. Furthermore, as siderophores produced in deep-sea hydrothermal plumes are not subjected to photo-degradation, a major break-down mechanism of siderophores in the photic zone[31],

they may disperse away from the plume and contribute to the pool of strong Fe-binding ligands (L1-type) found in the deep oceans[11,32,33], thus enhancing the effects of "microbial Fe pump" in the deep oceans.

The molecular and geochemical evidence presented here points to microbial scavenging of Fe from freshly precipitated minerals in hydrothermal plumes as a mechanism by which inorganic Fe is transferred to the organic phase. This process should be enhanced in deep-sea hydrothermal plumes where microbes are stimulated by energy-rich electron donors (sulfur[34,35], methane[36], ammonia[37], and H_2[34]) that fuel microbial growth via autotrophy and subsequent heterotrophy (Fig. 5). The few data points that are available suggest that the interplay between Fe, organic carbon, and microorganisms is distinct at different hydrothermal systems[9-11], suggesting that the fate of hydrothermal Fe in the deep sea is governed by dynamic biogeochemical factors. Important details remain unresolved; we are currently unable to quantify the strength of this microbial Fe pump or determine the nature of the siderophores or other ligands involved. Due to the uncultivated nature of the microbial populations discussed here, biochemical knowledge of the proteins encoded by the putative Fe-related genes is limited. However, recent evidence of extensive organically-complexed Fe in dispersing hydrothermal plumes[13,14] highlights the need to explore these questions further. The ubiquitous and culturable nature of *Alteromonas macleodii*, one of the siderophore utilizers identified here, along with advances in analytical methods for probing Fe and carbon speciation in the environment, suggests that addressing such questions is within reach.

Methods

Sample information. Seawater samples were collected on three cruises abroad R/V *New Horizon* in 2004 and 2005 from the Guaymas Basin hydrothermal plume and background as described previously[34,38]. Metadata and physical/chemical characteristics of each sample are presented in detail in recent publications[21,34] and also listed in supplementary Table 1.

Metatranscriptomics. Nucleic acids extraction and sequencing were done as described previously[21,34,38]. The Illumina metatranscriptomic datasets from plume and background samples were used for *de novo* assembly independently[20]. In brief, cDNA reads were first de-replicated by removing identical reads then quality trimmed with Sickle (score > 30). These de-replicated and trimmed cDNA reads were assembled by Velvet (1.2.01) and processed using the transcriptomic assembler Oases 0.2.04[39]. Abundance of transcripts was determined by mapping all cDNA reads to the assembled fragments using BWA with default settings[40] and normalizing to the length of each gene. Assembled contigs were submitted to the DOE Joint Genome Institutes (JGI) Integrated Microbial Genomes website (http://img.jgi.doe.gov/cgi-bin/w/main.cgi) for gene calling and annotation.

Identification of Fe uptake transcripts. We searched all annotated genes on assembled GB mRNA transcripts against a published Fe uptake gene database (E value < 10^{-20})[17,18]. We then compared positive hits to the non-redundant NCBI protein database. Only those that had top hits to Fe uptake genes were considered to be involved in Fe uptake. These identified Fe uptake genes were divided into different pathways as described previously[17]. To estimate the relative abundance of transcripts

for each pathway of Fe uptake, we mapped all of the cDNA reads to each Fe uptake gene in the GB assembly as well as available databases[17,18].

GBAlt analysis. We searched all annotated genes on assembled GB mRNA transcripts using all of *Alteromonas macleodii* genes (E value < 10^{-20})[22]. We then compared positive hits to the non-redundant NCBI protein database. Only those that had top hits to *A. macleodii* genes were considered to be GBAlt. Gene similarities between GBAlt and two ecotypes (ATCC 27126 and AltDE) of *Alteromonas* bacteria[22] were analyzed by a BLASTn analysis (bit score > 50). Function of TonB-dependent transporters was predicted and classified based on the database and approach as described previously[41], while classification of GBAlt ABC transporter function was analyzed based on the top hit in a BLASTx analysis.

Phylogenetic relationship of GBAlt was analyzed based on the 16S rRNA sequence recovered by the EMIRGE program[42] from GB transcriptomes and previous published clone sequences at the same research area[38]. 16S rRNA sequences were aligned in Greengenes[43] and imported into ARB for phylogenetic analyses using maximum likelihood (RaxML)[44]. Phylogenetic trees of two housekeeping genes encoding the β subunits of DNA gyrase (*gyrB*) and RNA polymerase (*rpoB*) were also constructed by maximum likelihood to evaluate the phylogenetic relationship of GBAlt with other ecotypes of *Alteromonas* bacteria[45].

Phylogenetic relationships of 16S rRNA (Supplementary Fig. 3) and two housekeeping genes encoding the β subunits of DNA gyrase (*gyrB*) and RNA polymerase (*rpoB*) clearly show that the major active species of the GB plume *A. macleodii* population (GBAlt) are more closely related to the "surface ecotype" rather than the "deep ecotype" of *A. macleodii* (Supplementary Fig. 3). Genome comparison

further indicates that GBAlt (2549 mRNAs, ~1.2 Mb) shares 95.1% average sequence identity with the surface ecotype (ATCC 27126), and 91.8% with the deep ecotype of *A. macleodii* (AltDE) (Supplementary Fig. 4). The higher sequence similarity between GBAlt and surface ecotype demonstrates that previously observed biogeographic distribution patterns of *A. macleodii* might be not suitable for the species present at deep-sea hydrothermal vents, including GBAlt and several isolates from hydrothermal vents (Supplementary Fig. 3).

Thermodynamic modeling. Equilibrium thermodynamic reaction path modeling was used to predict Fe mineral precipitation, chemical concentrations, and activity coefficients resulting from the mixing of seawater with Guaymas Basin end member vent fluid (Supplementary Fig. 5). Our approach follows those of previous studies[46,47]. Our Guaymas plume model was described in detail in Anantharaman et al.[34] and builds on the specific plume model implementation of Breier et al.[12]. The endmember chemical concentrations and implementation used in this model are the same as that for Anantharaman et al.[34], with the exception of a subset of assumptions which were added to more accurately predict mineral formation following our approach in Breier et al.[12]. The following is a brief description of the aspects of this model pertinent to this study; interested readers are referred to Anantharaman et al.[34] for more details.

The Guaymas plume reaction path is modeled through a mixing process that ends at a vent fluid to seawater dilution of 1 part in 10,000, representing the dilution achieved at the non-buoyant plume heights sampled in this study. Vent fluid composition was based on measurements made in 1982 and 2000 [28,48]. *In situ* pH was calculated from measurements of pH at 25 ° C using an equilibrium reaction path model that increased

the temperature of the measured fluid to the original vent fluid temperature. Background seawater dissolved O_2 concentration was based on previous measurements reported for Guaymas basin hydrothermal plumes[49]. Note, the available data predates this study; actual vent chemistry during this study may have differed.

Reaction path modeling was performed with REACT, part of the Geochemist's Workbench package[50]. Conductive cooling was neglected and mixture temperatures were a strict function of conservative end-member mixing. Precipitated minerals were allowed to dissolve and their constituents to re-precipitate based on thermodynamic equilibrium constraints. Thermodynamic data was predicted by SUPCRT95[51] for the temperature range of 1-425° C (specifically 1, 25, 60, 100, 225, 290, 350, and 425° C) and a pressure of 500 bar, a pressure and temperature range that encompasses all known deep sea vents. SUPCRT95 uses previously published thermodynamic data for minerals, gases, and aqueous species[52-56]. Thermodynamic data for pyrolusite, bixbyite, hausmannite, marcasite, and $Fe(OH)_3$ were added for our study[57,58]. The B-dot activity model was used[59,60]. Temperature dependent activity coefficients were used for aqueous CO_2 and water in an NaCl solution[50,61,62]. A general limitation of REACT is that it does not predict the thermodynamic behavior of solid solutions. Thus minerals such as sphalerite, pyrrhotite, chalcopyrite, and isocubanite are treated as separate phases with ideal stoichiometries. This may influence the predicted plume mineral assemblage.

In Anantharaman et al.[34], we suppressed all aqueous phase redox couples in order to estimate upper limit constraints on potential chemosynthetic metabolic energy. In this case, we use these same assumptions but because of our specific interest in Fe speciation in this study we have added additional assumptions related to mineral formation following Breier et al.[12] The precipitation of hematite was suppressed to

allow Fe hydroxide to precipitate on the basis that the latter is a closer approximation than the former to the more common amorphous Fe oxyhydroxides, which precipitate preferentially due to kinetic effects. The precipitation of Mg bearing minerals, and silicates, with the exception of amorphous silica, were also suppressed for simplicity. Some in this group have been found as minor plume constituents, others such as quartz appear kinetically inhibited; but in any case, the suppression of this group does not influence the precipitation of the minerals of interest in this study. Precipitated minerals were allowed to dissolve and their constituents to re-precipitate based on thermodynamic equilibrium constraints.

Bulk Elemental Analysis. Particulate filter samples were completely digested in 30 mL acid cleaned perfluoroalkoxy vials (Savillex) using the following procedure based on Bowie et al.[63]. The 0.2 μm, 142 mm diameter, polyethersulfone membrane filters (SUPOR, Pall Corporation) were split into 1/8 sections. Each filter split was added to a digestion vials with 2 ml concentrated nitric acid. The vials were capped and heated at 110° C for 4 hrs. After cooldown 0.5 mL of concentrated hydrofluoric acid was added to each vial. The vials were capped and heated at 110° C for 4 hrs. The vials were then uncapped and heated at 120° C to dryness. An additional 100 μL of concentrated nitric acid was added and similarly taken to dryness to facilitate evaporation of the hydrofluoric acid. After cool down, the digested sample was taken back into solution by adding 3 mL of a 3% nitric acid matrix. The vials were capped and heated for 1 hour at 60° C. This process resulted in the complete digestion of visible particles and in most cases the filter, in the few cases where residual filter material (< 1% of the whole filter) remained it was removed by filtration of the digest solution. All acids were trace metal grade (Optima, Fisher Scientific). Vials were

heated in a temperature-controlled hot plate (Qblock, Questron Technologies). Aliquots of sample digest, at a 1:10 dilution, were analyzed for Fe, Mn, Fe, Al, Ti, P, Zn, Ni, Cu and U by inductively coupled plasma optical emission spectrometry on a Varian 730-ES axial spectrometer by Activation Laboratories. External standards were used for instrument calibration. Digestion and analysis were both monitored by processing portions of the basalt geostandard BHVO-1[64] with these samples (Supplementary Table 2).

STXM and C XANES Spectroscopy. Scanning transmission X-ray microscopy (STXM) and C 1s X-ray absorption near edge structure (XANES) spectroscopy were performed at the Advanced Light Source, Lawrence Berkeley National Laboratory, Berkeley, CA, USA, on beamline 5.3.2.2[65]. Guaymas Basin plume particles were re-suspended from the original PES filter by gentle shaking in 0.5 mL of purified water. From this suspension, ~ 1 µL was deposited on a silicon nitride membrane (Silson Ltd.) and air-dried. This preparation resulted in dispersed particles with no sea salt precipitates. Optical density (OD) images were made from X-ray images recorded at energies just below and at the C 1s (280, 305 eV), N 1s (395, 401.5 eV), Mn 2p (635, 643 eV), and Fe 2p (700, 709.5 eV) absorption edges. The Fe 2p 709.5 eV image will preferentially display Fe(III) if present. Fe 2p images were also collected at 707.6 eV to test the sample for Fe(II). The patterns observed for 709.5 eV and 707.6 eV images revealed the same pattern of Fe in the particles with differing optical densities. Therefore, only the elemental maps derived from the 709.5 eV images are displayed in Supplementary Fig.6. Carbon 1s XANES spectra from regions of interest were obtained from image sequences (called stacks) collected at energies spanning the absorption edge (280-340 eV for C). Theoretical spatial and spectral resolutions were 20 nm and ± 0.1 eV, respectively. All measurements were performed at ambient

temperature and < 1 atm He. Calibration at the C 1s edge was accomplished with the 3s (292.74 eV) and 3p (294.96 eV) Rydberg transitions of gaseous CO_2. All STXM data processing was carried out with the IDL *aXis2000* software package (http://unicorn.mcmaster.ca/aXis2000.html). All XANES data processing was done in program *Athena*.

X-ray Microprobe and Fe 1s XANES Spectroscopy. A small (~ 1.5 cm^2) portion of the original PES filter, obtained using a ceramic scalpel, was mounted on an aluminum sample holder. The remaining sample was stored frozen. Data collection at the ALS beamline 10.3.2[66] had the following task flow for these filter-bound plume particles: X-ray fluorescence (XRF) mapping at multiple energies to determine the spatial distribution of elements in the particles within a region of interest; and Fe 1s XANES spectroscopy measurements at specific locations (i.e. particles or particle aggregates) within the region of interest.

The distribution of Fe, Mn, Ca, and other elements was measured in an area 0.995 × 1.865 mm^2 by microprobe XRF using a 7-element Ge solid-state fluorescence detector (Canberra) with a pixel size of 5 × 5 μm^2. XRF mapping included: (1) an "As map" with incident energy set to PbL_3-50, or 12,985 eV, that provided Fe, Ni, Cu, Zn, and As distributions; (2) a "Mn map" with incident energy set to FeK-50, or 7062 eV, that provided Mn distribution without interference from Fe Kα fluorescence emission; and (3) a "V map" was generated by subtracting a VK-50, or 5415 eV map from a VK+100, or 5565 eV to distinguish V Kα from Ti Kβ fluorescence emission. Light elements, Si, S, Cl, K, and Ca, were obtained from the lowest energy map collected. Individual XRF maps were deadtime corrected, aligned, and channels of interest were added to a single composite map using custom beamline software[66].

The composite XRF map was used to locate particles for Fe 1s XANES spectroscopy. The monochromator energy calibration was set with the inflection point of a scan of Fe foil at 7110.75 eV. Iron XANES were conducted in "quick" mode using the fluorescence detector. Individual scans of the monochromator required 30 s, and were repeated up to 60 times. Data scans collected at the same sample location were examined for changes in line-shape and peak position, and no photon-induced sample damage was observed. Spectra were deadtime corrected, energy calibrated, and averaged using custom beamline software[66]. The software program *Athena* was used to perform pre-edge subtraction and post-edge normalization[67]. Normalized spectra were subjected to linear combination fitting (LCF) with reference spectra using custom beamline software[66] as described in previous study[12]. The Fe reference spectra database used has 94 entries[68-70].

References

1 Boyd, P. W. & Ellwood, M. J. The biogeochemical cycle of iron in the ocean. *Nat. Geosci.* **3**, 675-682 (2010).

2 Smetacek, V. *et al.* Deep carbon export from a Southern Ocean iron-fertilized diatom bloom. *Nature* **487**, 313-319 (2012).

3 Sandy, M. & Butler, A. Microbial iron acquisition: marine and terrestrial siderophores. *Chem. Rev.* **109**, 4580-4595 (2009).

4 Crichton, R. *Iron metabolism : from molecular mechanisms to clinical consequences*. 3rd edn, (John Wiley & Sons, 2009).

5 Escolar, L., Perez-Martin, J. & de Lorenzo, V. Opening the iron box: transcriptional metalloregulation by the Fur protein. *J. Bacteriol.* **181**, 6223-6229 (1999).

6 Maranger, R., Bird, D. F. & Price, N. M. Iron acquisition by photosynthetic marine phytoplankton from ingested bacteria. *Nature* **396**, 248-251 (1998).

7 Elderfield, H. & Schultz, A. Mid-ocean ridge hydrothermal fluxes and the chemical composition of the ocean. *Annu. Rev. Earth Pl. Sci.* **24**, 191-224 (1996).

8 Toner, B. M., Marcus, M. A., Edwards, K. J., Rouxel, O. & German, C. R. Measuring the Form of Iron in Hydrothermal Plume Particles. *Oceanography* **25**, 209-212 (2012).

9 Toner, B. M. *et al.* Preservation of iron(II) by carbon-rich matrices in a hydrothermal plume. *Nat. Geosci.* **2**, 197-201 (2009).

10 Bennett, S. A. *et al.* The distribution and stabilisation of dissolved Fe in deep-sea hydrothermal plumes. *Annu. Rev. Earth Pl. Sci.* **270**, 157-167 (2008).

11 Sander, S. G. & Koschinsky, A. Metal flux from hydrothermal vents increased by organic complexation. *Nat. Geosci.* **4**, 145-150 (2011).

12 Breier, J. A. *et al.* Sulfur, sulfides, oxides and organic matter aggregated in submarine hydrothermal plumes at 9 °C 50 ' N East Pacific Rise. *Geochim. Cosmochim. Ac.* **88**, 216-236 (2012).

13 Nishioka, J., Obata, H. & Tsumune, D. Evidence of an extensive spread of hydrothermal dissolved iron in the Indian Ocean. *Earth Planet Sci. Lett.* **361**, 26-33 (2013).

14 Klunder, M. B., Laan, P., Middag, R., de Baar, H. J. W. & Bakker, K. Dissolved iron in the Arctic Ocean: Important role of hydrothermal sources, shelf input and scavenging removal. *J. Geophys Res.-Oceans* **117** (2012).

15 Wu, J. F., Wells, M. L. & Rember, R. Dissolved iron anomaly in the deep tropical-subtropical Pacific: Evidence for long-range transport of hydrothermal iron. *Geochim. Cosmochim. Ac.* **75**, 460-468 (2011).

16 Tagliabue, A. *et al.* Hydrothermal contribution to the oceanic dissolved iron inventory. *Nat. Geosci.* **3**, 252-256 (2010).

17 Toulza, E., Tagliabue, A., Blain, S. & Piganeau, G. Analysis of the Global Ocean Sampling (GOS) Project for Trends in Iron Uptake by Surface Ocean Microbes. *Plos One* **7**, e30931 (2012).

18 Hopkinson, B. M. & Barbeau, K. A. Iron transporters in marine prokaryotic genomes and metagenomes. *Environ. Microbiol.* **14**, 114-128 (2012).

19 Dick, G. J. *et al.* The microbiology of deep-sea hydrothermal vent plumes: ecological and biogeographic linkages to seafloor and water column habitats. *Front. Microbiol.* **4**, 124 (2013).

20 Baker, B. J. *et al.* Community transcriptomic assembly reveals microbes that contribute to deep-sea carbon and nitrogen cycling. *ISME J.* (in press) doi: 10.1038/ismej.2013.85 (2013).
21 Lesniewski, R. A., Jain, S., Anantharaman, K., Schloss, P. D. & Dick, G. J. The metatranscriptome of a deep-sea hydrothermal plume is dominated by water column methanotrophs and chemolithotrophs. *ISME J.* **6**, 2257-2268 (2012).
22 Ivars-Martinez, E. *et al.* Comparative genomics of two ecotypes of the marine planktonic copiotroph Alteromonas macleodii suggests alternative lifestyles associated with different kinds of particulate organic matter. *ISME J.* **2**, 1194-1212 (2008).
23 Vraspir, J. M. & Butler, A. Chemistry of marine ligands and siderophores. *Ann. Rev. Mar. Sci.* **1**, 43-63 (2009).
24 Velasquez, I. *et al.* Detection of hydroxamate siderophores in coastal and Sub-Antarctic waters off the South Eastern Coast of New Zealand. *Mar. Chem.* **126**, 97-107 (2011).
25 Mawji, E. *et al.* Hydroxamate siderophores: occurrence and importance in the Atlantic Ocean. *Environ. Sci. Technol.* **42**, 8675-8680 (2008).
26 Trick, C. G. Hydroxamate-Siderophore Production and Utilization by Marine Eubacteria. *Curr. Microbiol.* **18**, 375-378 (1989).
27 Holt, P. D., Reid, R. R., Lewis, B. L., Luther, G. W. & Butler, A. Iron(III) coordination chemistry of alterobactin A: A siderophore from the marine bacterium Alteromonas luteoviolacea. *Inorg. Chem.* **44**, 7671-7677 (2005).
28 Von Damm, K. L., Edmond, J. M., Measures, C. I. & Grant, B. Chemistry of Submarine Hydrothermal Solutions at Guaymas Basin, Gulf of California. *Geochim. Cosmochim. Ac.* **49**, 2221-2237 (1985).
29 Boström, K. & Peterson, M. N. A. The origin of aluminum-poor ferromanganoan sediments in areas of high heat flow on the East Pacific Rise. *Mar. Geol.* **7**, 427-477 (1969).
30 Kraemer, S. M., Butler, A., Borer, P. & Cervini-Silva, J. Siderophores and the dissolution of iron-bearing minerals in marine systems. *Rev. Mineral. Geochem.* **59**, 53-84 (2005).
31 Barbeau, K., Rue, E. L., Bruland, K. W. & Butler, A. Photochemical cycling of iron in the surface ocean mediated by microbial iron(III)-binding ligands. *Nature* **413**, 409-413 (2001).
32 Ibisanmi, E., Sander, S. G., Boyd, P. W., Bowie, A. R. & Hunter, K. A. Vertical distributions of iron-(III) complexing ligands in the Southern Ocean. *Deep-Sea Res. II* **58**, 2113-2125 (2011).
33 Kondo, Y., Takeda, S. & Furuya, K. Distinct trends in dissolved Fe speciation between shallow and deep waters in the Pacific Ocean. *Mar. Chem.* **134**, 18-28 (2012).
34 Anantharaman, K., Breier, J. A., Sheik, C. S. & Dick, G. J. Evidence for hydrogen oxidation and metabolic plasticity in widespread deep-sea sulfur-oxidizing bacteria. *Proc. Natl. Acad. Sci. U S A* **110**, 330-335 (2013).
35 Sheik, C. S., Jain, S. & Dick, G. J. Metabolic flexibility of enigmatic SAR324 revealed through metagenomics and metatranscriptomics. *Environ. Microbiol.* (in press) doi: 10.1111/1462-2920.12165 (2013).
36 Li, M., Jain, S., Baker, B. J., Taylor, C. A. & Dick, G. J. Novel hydrocarbon monooxygenase genes in the metatranscriptome of a natural deep-sea

hydrocarbon plume. *Environ. Microbiol.* (in press) doi: 10.1111/1462-2920.12182 (2013).

37 Baker, B. J., Lesniewski, R. A. & Dick, G. J. Genome-enabled transcriptomics reveals archaeal populations that drive nitrification in dee-sea hydrothermal plume. *ISME J.* **6**, 2269-2279 (2012).

38 Dick, G. J. & Tebo, B. M. Microbial diversity and biogeochemistry of the Guaymas Basin deep-sea hydrothermal plume. *Environ. Microbiol.* **12**, 1334-1347 (2010).

39 Schulz, M. H., Zerbino, D. R., Vingron, M. & Birney, E. Oases: robust de novo RNA-seq assembly across the dynamic range of expression levels. *Bioinformatics* **28**, 1086-1092 (2012).

40 Li, H. & Durbin, R. Fast and accurate short read alignment with Burrows-Wheeler transform. *Bioinformatics* **25**, 1754-1760 (2009).

1 Boyd, P. W. & Ellwood, M. J. The biogeochemical cycle of iron in the ocean. *Nat Geosci* **3**, 675-682, doi:Doi 10.1038/Ngeo964 (2010).

2 Smetacek, V. *et al.* Deep carbon export from a Southern Ocean iron-fertilized diatom bloom. *Nature* **487**, 313-319, doi:Doi 10.1038/Nature11229 (2012).

3 Sandy, M. & Butler, A. Microbial iron acquisition: marine and terrestrial siderophores. *Chem Rev* **109**, 4580-4595, doi:10.1021/cr9002787 (2009).

4 Crichton, R. *Iron metabolism : from molecular mechanisms to clinical consequences*. 3rd edn, (John Wiley & Sons, 2009).

5 Escolar, L., Perez-Martin, J. & de Lorenzo, V. Opening the iron box: transcriptional metalloregulation by the Fur protein. *J Bacteriol* **181**, 6223-6229 (1999).

6 Maranger, R., Bird, D. F. & Price, N. M. Iron acquisition by photosynthetic marine phytoplankton from ingested bacteria. *Nature* **396**, 248-251 (1998).

7 Elderfield, H. & Schultz, A. Mid-ocean ridge hydrothermal fluxes and the chemical composition of the ocean. *Annu Rev Earth Pl Sc* **24**, 191-224 (1996).

8 Toner, B. M., Marcus, M. A., Edwards, K. J., Rouxel, O. & German, C. R. Measuring the Form of Iron in Hydrothermal Plume Particles. *Oceanography* **25**, 209-212 (2012).

9 Toner, B. M. *et al.* Preservation of iron(II) by carbon-rich matrices in a hydrothermal plume. *Nat Geosci* **2**, 197-201, doi:Doi 10.1038/Ngeo433 (2009).

10 Bennett, S. A. *et al.* The distribution and stabilisation of dissolved Fe in deep-sea hydrothermal plumes. *Earth and Planetary Science Letters* **270**, 157-167, doi:DOI 10.1016/j.epsl.2008.01.048 (2008).

11 Sander, S. G. & Koschinsky, A. Metal flux from hydrothermal vents increased by organic complexation. *Nature Geoscience* **4**, 145-150, doi:Doi 10.1038/Ngeo1088 (2011).

12 Breier, J. A. *et al.* Sulfur, sulfides, oxides and organic matter aggregated in submarine hydrothermal plumes at 9 degrees 50 ' N East Pacific Rise. *Geochim Cosmochim Ac* **88**, 216-236, doi:DOI 10.1016/j.gca.2012.04.003 (2012).

13 Nishioka, J., Obata, H. & Tsumune, D. Evidence of an extensive spread of hydrothermal dissolved iron in the Indian Ocean. *Earth Planet Sc Lett* **361**, 26-33 (2013).
14 Klunder, M. B., Laan, P., Middag, R., de Baar, H. J. W. & Bakker, K. Dissolved iron in the Arctic Ocean: Important role of hydrothermal sources, shelf input and scavenging removal. *J Geophys Res-Oceans* **117** (2012).
15 Wu, J. F., Wells, M. L. & Rember, R. Dissolved iron anomaly in the deep tropical-subtropical Pacific: Evidence for long-range transport of hydrothermal iron. *Geochim Cosmochim Ac* **75**, 460-468 (2011).
16 Tagliabue, A. *et al.* Hydrothermal contribution to the oceanic dissolved iron inventory. *Nature Geoscience* **3**, 252-256, doi:Doi 10.1038/Ngeo818 (2010).
17 Toulza, E., Tagliabue, A., Blain, S. & Piganeau, G. Analysis of the Global Ocean Sampling (GOS) Project for Trends in Iron Uptake by Surface Ocean Microbes. *Plos One* **7**, doi:ARTN e30931 DOI 10.1371/journal.pone.0030931 (2012).
18 Hopkinson, B. M. & Barbeau, K. A. Iron transporters in marine prokaryotic genomes and metagenomes. *Environ Microbiol* **14**, 114-128, doi:Doi 10.1111/J.1462-2920.2011.02539.X (2012).
19 Dick, G. J. *et al.* The microbiology of deep-sea hydrothermal vent plumes: ecological and biogeographic linkages to seafloor and water column habitats. *Front Microbiol*, doi:10.3389/fmicb.2013.00124 (2013).
20 Baker, B. J. *et al.* Community transcriptomic assembly reveals microbes that contribute to deep-sea carbon and nitrogen cycling. *ISME Journal* (2013).
21 Lesniewski, R. A., Jain, S., Anantharaman, K., Schloss, P. D. & Dick, G. J. The metatranscriptome of a deep-sea hydrothermal plume is dominated by water column methanotrophs and chemolithotrophs. *Isme J* **6**, 2257-2268 (2012).
22 Ivars-Martinez, E. *et al.* Comparative genomics of two ecotypes of the marine planktonic copiotroph Alteromonas macleodii suggests alternative lifestyles associated with different kinds of particulate organic matter. *Isme Journal* **2**, 1194-1212, doi:Doi 10.1038/Ismej.2008.74 (2008).
23 Vraspir, J. M. & Butler, A. Chemistry of marine ligands and siderophores. *Ann Rev Mar Sci* **1**, 43-63 (2009).
24 Velasquez, I. *et al.* Detection of hydroxamate siderophores in coastal and Sub-Antarctic waters off the South Eastern Coast of New Zealand. *Mar Chem* **126**, 97-107 (2011).
25 Mawji, E. *et al.* Hydroxamate siderophores: occurrence and importance in the Atlantic Ocean. *Environ Sci Technol* **42**, 8675-8680 (2008).
26 Trick, C. G. Hydroxamate-Siderophore Production and Utilization by Marine Eubacteria. *Curr Microbiol* **18**, 375-378 (1989).
27 Holt, P. D., Reid, R. R., Lewis, B. L., Luther, G. W. & Butler, A. Iron(III) coordination chemistry of alterobactin A: A siderophore from the marine bacterium Alteromonas luteoviolacea. *Inorg Chem* **44**, 7671-7677 (2005).
28 Von Damm, K. L., Edmond, J. M., Measures, C. I. & Grant, B. Chemistry of Submarine Hydrothermal Solutions at Guaymas Basin, Gulf of California.

Geochim Cosmochim Ac **49**, 2221-2237, doi:Doi 10.1016/0016-7037(85)90223-6 (1985).

29 Boström, K. & Peterson, M. N. A. The origin of aluminum-poor ferromanganoan sediments in areas of high heat flow on the East Pacific Rise. *Marine Geology* **7**, 427-477 (1969).

30 Kraemer, S. M., Butler, A., Borer, P. & Cervini-Silva, J. Siderophores and the dissolution of iron-bearing minerals in marine systems. *Rev Mineral Geochem* **59**, 53-84, doi:Doi 10.2138/Rmg.2005.59.4 (2005).

31 Barbeau, K., Rue, E. L., Bruland, K. W. & Butler, A. Photochemical cycling of iron in the surface ocean mediated by microbial iron(III)-binding ligands. *Nature* **413**, 409-413, doi:10.1038/35096545 (2001).

32 Ibisanmi, E., Sander, S. G., Boyd, P. W., Bowie, A. R. & Hunter, K. A. Vertical distributions of iron-(III) complexing ligands in the Southern Ocean. *Deep-Sea Res Pt Ii* **58**, 2113-2125 (2011).

33 Kondo, Y., Takeda, S. & Furuya, K. Distinct trends in dissolved Fe speciation between shallow and deep waters in the Pacific Ocean. *Mar Chem* **134**, 18-28 (2012).

34 Anantharaman, K., Breier, J. A., Sheik, C. S. & Dick, G. J. Evidence for hydrogen oxidation and metabolic plasticity in widespread deep-sea sulfur-oxidizing bacteria. *Proc Natl Acad Sci U S A* **110**, 330-335, doi:10.1073/pnas.1215340110 (2013).

35 Sheik, C. S., Jain, S. & Dick, G. J. Metabolic flexibility of enigmatic SAR324 revealed through metagenomics and metatranscriptomics. *Environ Microbiol* (2013).

36 Li, M., Jain, S., Baker, B. J., Taylor, C. A. & Dick, G. J. Novel hydrocarbon monooxygenase genes in the metatranscriptome of a natural deep-sea hydrocarbon plume. *Environ Microbiol* (2013).

37 Baker, B. J., Lesniewski, R. A. & Dick, G. J. Genome-enabled transcriptomics reveals archaeal populations that drive nitrification in dee-sea hydrothermal plume. *Isme J* **6**, 2269-2279 (2012).

38 Dick, G. J. & Tebo, B. M. Microbial diversity and biogeochemistry of the Guaymas Basin deep-sea hydrothermal plume. *Environ Microbiol* **12**, 1334-1347, doi:10.1111/j.1462-2920.2010.02177.x (2010).

39 Schulz, M. H., Zerbino, D. R., Vingron, M. & Birney, E. Oases: robust de novo RNA-seq assembly across the dynamic range of expression levels. *Bioinformatics* **28**, 1086-1092, doi:10.1093/bioinformatics/bts094 bts094 [pii] (2012).

40 Li, H. & Durbin, R. Fast and accurate short read alignment with Burrows-Wheeler transform. *Bioinformatics* **25**, 1754-1760, doi:DOI 10.1093/bioinformatics/btp324 (2009).

41 Tang, K., Jiao, N., Liu, K., Zhang, Y. & Li, S. Distribution and functions of TonB-dependent transporters in marine bacteria and environments: implications for dissolved organic matter utilization. *Plos One* **7**, e41204, doi:10.1371/journal.pone.0041204 (2012).

42 Miller, C. S., Baker, B. J., Thomas, B. C., Singer, S. W. & Banfield, J. F. EMIRGE: reconstruction of full-length ribosomal genes from microbial community short read sequencing data. *Genome Biol* **12**, R44, doi:10.1186/gb-2011-12-5-r44 (2011).

43 DeSantis, T. Z. *et al.* Greengenes, a chimera-checked 16S rRNA gene database and workbench compatible with ARB. *Appl Environ Microbiol* **72**, 5069-5072, doi:10.1128/AEM.03006-05 (2006).
44 Ludwig, W. *et al.* ARB: a software environment for sequence data. *Nucleic Acids Res* **32**, 1363-1371, doi:10.1093/nar/gkh293 (2004).
45 Ivars-Martinez, E. *et al.* Biogeography of the ubiquitous marine bacterium Alteromonas macleodii determined by multilocus sequence analysis. *Mol Ecol* **17**, 4092-4106 (2008).
46 Bowers, T. S., Vondamm, K. L. & Edmond, J. M. Chemical Evolution of Mid-Ocean Ridge Hot Springs. *Geochim Cosmochim Ac* **49**, 2239-2252 (1985).
47 Janecky, D. R. & Seyfried, W. E. Formation of Massive Sulfide Deposits on Oceanic Ridge Crests - Incremental Reaction Models for Mixing between Hydrothermal Solutions and Seawater. *Geochim Cosmochim Ac* **48**, 2723-2738 (1984).
48 Von Damm, K. L. *et al.* The Escanaba Trough, Gorda Ridge hydrothermal system: Temporal stability and subseafloor complexity. *Geochim Cosmochim Ac* **69**, 4971-4984 (2005).
49 Campbell, A. C. & Gieskes, J. M. Water Column Anomalies Associated with Hydrothermal Activity in the Guaymas Basin, Gulf of California. *Earth Planet Sc Lett* **68**, 57-72 (1984).
50 Bethke, C. M. *Geochemical and biogeochemical reaction modeling*. (Cambridge University Press, 2007).
51 Johnson, J. W., Oelkers, E. H. & Helgeson, H. C. Supcrt92 - a Software Package for Calculating the Standard Molal Thermodynamic Properties of Minerals, Gases, Aqueous Species, and Reactions from 1-Bar to 5000-Bar and 0-Degrees-C to 1000-Degrees-C. *Comput Geosci* **18**, 899-947 (1992).
52 Helgeson, H. C., Delany, J. M., Nesbitt, H. W. & Bird, D. K. Summary and Critique of the Thermodynamic Properties of Rock-Forming Minerals. *Am J Sci* **278**, 1-229 (1978).
53 Saccocia, P. J. & Seyfried, W. E. The Solubility of Chlorite Solid-Solutions in 3.2 Wt-Percent Nacl Fluids from 300-400-Degrees-C, 500 Bars. *Geochim Cosmochim Ac* **58**, 567-585 (1994).
54 Shock, E. L., Helgeson, H. C. & Sverjensky, D. A. Calculation of the Thermodynamic and Transport-Properties of Aqueous Species at High-Pressures and Temperatures - Standard Partial Molal Properties of Inorganic Neutral Species. *Geochim Cosmochim Ac* **53**, 2157-2183 (1989).
55 Shock, E. L., Sassani, D. C., Willis, M. & Sverjensky, D. A. Inorganic species in geologic fluids: Correlations among standard molal thermodynamic properties of aqueous ions and hydroxide complexes. *Geochim Cosmochim Ac* **61**, 907-950 (1997).
56 Sverjensky, D. A., Shock, E. L. & Helgeson, H. C. Prediction of the thermodynamic properties of aqueous metal complexes to 1000 degrees C and 5 kb. *Geochim Cosmochim Ac* **61**, 1359-1412 (1997).
57 Robie, R. A., Hemingway, B. S. & Fisher, J. R. in *U.S. Geological Survey bulletin 1452* (U.S. Geological Survey, 1979).
58 Wagman, D. D. *et al.* (American Chemical Society and the American Institute of Physics for the National Bureau of Standards, 1982).
59 Helgeson, H. C. Thermodynamics of Hydrothermal Systems at Elevated Temperatures and Pressures. *Am J Sci* **267**, 729-& (1969).

60 Helgeson, H. C., Kirkham, D. H. & Flowers, G. C. Theoretical Prediction of the Thermodynamic Behavior of Aqueous-Electrolytes at High-Pressures and Temperatures .4. Calculation of Activity-Coefficients, Osmotic Coefficients, and Apparent Molal and Standard and Relative Partial Molal Properties to 600-Degrees-C and 5 Kb. *Am J Sci* **281**, 1249-1516 (1981).
61 Drummond, S. E. *Boiling and mixing of hydrothermal fluids: chemical effects on mineral precipitation* Ph.D. thesis, Pennsylvania State University, (1981).
62 Cleverley, J. S. & Bastrakov, E. N. K2GWB: Utility for generating thermodynamic data files for The Geochemist's Workbench (R) at 0-1000 degrees C and 1-5000 bar from UT2K and the UNITHERM database. *Comput Geosci* **31**, 756-767 (2005).
63 Bowie, A. R., Townsend, A. T., Lannuzel, D., Remenyi, T. A. & van der Merwe, P. Modern sampling and analytical methods for the determination of trace elements in marine particulate material using magnetic sector inductively coupled plasma-mass spectrometry. *Anal Chim Acta* **676**, 15-27 (2010).
64 Govindaraju, K. 1994 compilation of working values and sample description for 383 geostandards. *Geostandards and Geoanalytical Research* **18**, 1639-4488 (1994).
65 Kilcoyne, A. L. D. *et al.* Interferometer-controlled scanning transmission X-ray microscopes at the Advanced Light Source. *J. Synchrotron Radiation* **10** (2003).
66 Marcus, M. A. *et al.* Beamline 10.3.2 at ALS: a hard X-ray microprobe for environmental and material sciences. *J. Synchrotron Rad.* **11**, 239-247 (2004).
67 Ravel, B. & Newville, M. Athena, Artemis, Hephaestus: data analysis for X-ray absorption spectroscopy using IFEFFIT. *Journal of Synchrotron Radiation* **12**, 537-541 (2005).
68 Marcus, M. A., Westphal, A. J. & Fakra, S. Classification of Fe-bearing species from K-edge XANES data using two-parameter correlation plots. *J Synchrotron Rad.* **15**, 463-468 (2008).
69 Toner, B. M. *et al.* Mineralogy of iron microbial mats from Loihi Seamount. *Frontiers in Microbiological Chemistry* **3**, 1-18, doi:doi:10.3389/fmicb.2012.00118 (2012).
70 Hansel, C. M. *et al.* Secondary mineralization pathways induced by dissimilatory iron reduction of ferrihydrite under advective flow. *Geochim. Cosmochim. Acta* **67**, 2977-2992 (2003).

End Notes

Acknowledgments. This project is funded by the Gordon and Betty Moore Foundation through grant GBMF 2609 to GJD/JAB/BMT and by the National Science Foundation through grants OCE 1029242 to GJD, and R2K grant OCE1038055 to JAB/BMT. We thank the University of Michigan Rackham Graduate School Faculty Research Fellowship Program for their support. We thank Professor Nianzhi Jiao, Dr. Kai Tang and Mr. Mo Chen at Xiamen University for helping the TonB gene function analysis and Dr. Brain Hopkinson at University of Georgia for providing iron transporter sequences. We thank Mr. Sunit Jain at University of Michigan for helping the bioinformatic analysis. We thank George Cody (Geophysical Laboratory) and Satish Myneni (Princeton University) for discussions regarding STXM data. We thank Matthew Marcus, Sirine Fakra, and David Kilcoyne for synchrotron support at the Advanced Light Source (BLs 10.3.2 and 5.3.2.2), and Sarah Bennett and Jeffry Sorensen for assistance in synchrotron data collection. The Advanced Light Source is supported by the Director, Office of Science, Office of Basic Energy Sciences, of the U.S. Department of Energy under Contract No. DE-AC02-05CH11231. Dr. Martin Tsz-ki Tsui (University of North Carolina at Greensboro) and members of Geomicrobiology lab at University of Michigan provided helpful comments and revisions to the manuscript.

Author contributions. M. Li and G.J. Dick designed research, analyzed data and wrote the paper; B.M. Toner performed spectromicroscopic measurements and wrote the paper; B. J. Baker did transcriptome *de novo* assembly and wrote the paper; J.A. Breier performed thermodynamic modeling, bulk elemental analysis and wrote the paper; C.S. Sheik performed 16S rRNA gene 454 pyrosequencing and wrote the paper.

Competing Financial Interests statement. The authors declare no conflict of interest.

Accession Codes. Sequences of cDNA Illumina reads for plume and background samples of this study have been deposited in the NCBI SRA database under accession numbers SRX134769 and SRX134768. The plume transcriptomic assembly sequences for this study have been deposited in JGI IMG/MER database under accession ID 23647000.

Figure Legends

Figure 1. Rank abundance of gene transcripts. The grey circles are genes of whole GB plume community and yellow triangles are genes for Fe uptake in the plume metatranscriptomic *de novo* assembly. The relative abundance of gene transcripts was normalized to the length of gene fragment and the total number of all transcripts. Representative genes involving in Fe transport are indicated.

Figure 2. Pathways of microbial Fe transport. The bar at the top shows the proportions of the GB hydrothermal plume transcripts assigned to each pathway, and the schematic below shows the corresponding pathways.

Figure 3. Relative abundance of Fe transcripts. Each bar indicates the proportion of transcripts assigned to different microbial groups for the five dominant pathways of Fe uptake, respectively.

Figure 4. Fe species obtained from modeling and Fe XANES spectroscopy. (a) Abundance of Fe species in mineral and aqueous phases in the GB plume (2 –10 °C) predicted by the thermodynamic modeling. The temperature of the plume samples collected in this study were 2.53 – 2.97 °C (indicated by the green bar). (b) Fe XANES spectra of Fe-bearing minerals in plume particles and (c) their observed distribution quantified by linear combination fitting of the spectromicroscopic data. In figure 4b, spot 0 to spot 3 are the iron XANES spectra collected from sample locations indicated in Supplementary Figure 7 panel (a), and vertical lines at 7129.5 eV, 7131 eV, and 7132 eV are to guide the eye; full spectra range is 7071.4 – 7367.6 eV.

Figure 5. Microbial Fe pump in deep-sea hydrothermal plumes. Uptake of Fe (primarily Fe(III)) is conducted by dominant chemosynthetic, methanotrophic, and

heterotrophic populations. Subsequent dispersal of Fe may occur as Fe-siderophore complexes or via whole cells or POC or DOC produced through cell lysis.

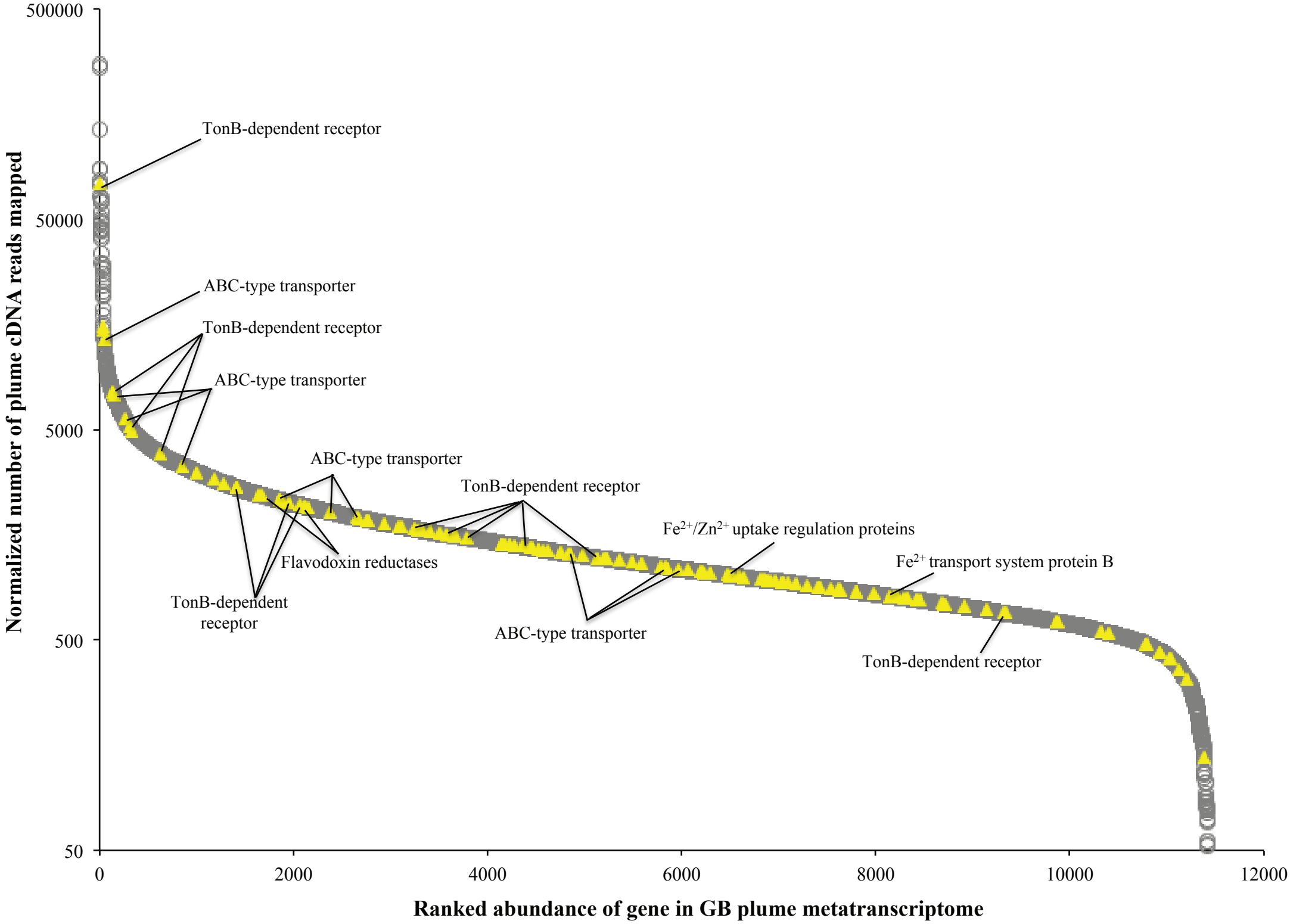
500000
50000
5000
500
50
0
2000
4000
6000
8000
10000
12000
Normalized number of plume cDNA reads mapped
Ranked abundance of gene in GB plume metatranscriptome
TonB-dependent receptor
ABC-type transporter
TonB-dependent receptor
ABC-type transporter
ABC-type transporter
TonB-dependent receptor
Fe2+/Zn2+ uptake regulation proteins
Fe2+ transport system protein B
Flavodoxin reductases
TonB-dependent receptor
ABC-type transporter
TonB-dependent receptor

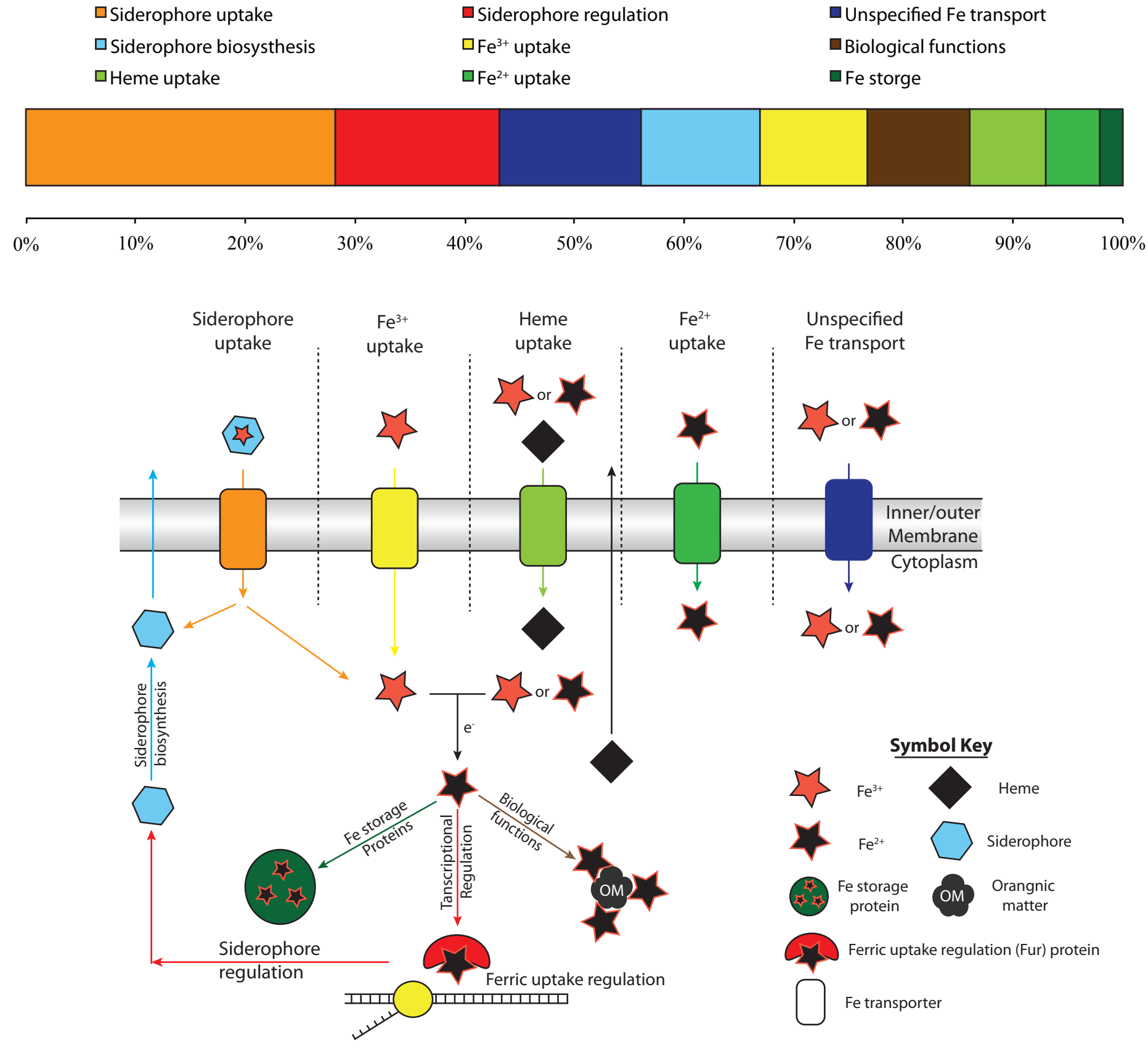
Siderophore uptake
Siderophore regulation
Unspecified Fe transport
Siderophore biosysthesis
Fe3+ uptake
Biological functions
Heme uptake
Fe2+ uptake
Fe storge
0%
10%
20%
30%
40%
50%
60%
70%
80%
90%
100%
Siderophore uptake
Fe3+ uptake
Heme uptake
Fe2+ uptake
Unspecified Fe transport
or
Inner/outer Membrane
Cytoplasm
Siderophore biosynthesis
e-
Fe storage Proteins
Tanscriptional Regulation
Biological functions
OM
Siderophore regulation
Ferric uptake regulation
Symbol Key
Fe3+
Heme
Fe2+
Siderophore
Fe storage protein
Orangnic matter
Ferric uptake regulation (Fur) protein
Fe transporter

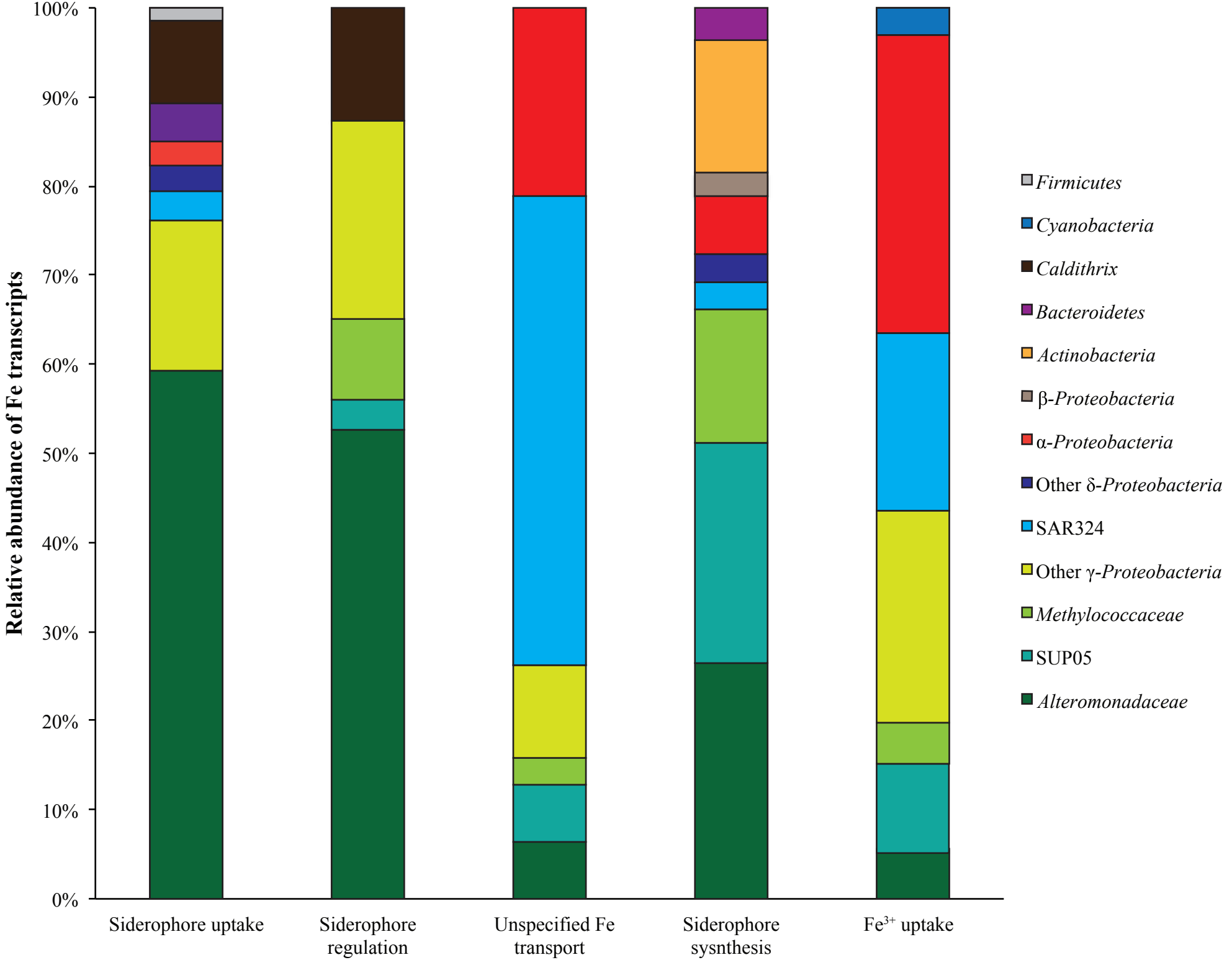
Relative abundance of Fe transcripts
100%
90%
80%
70%
60%
50%
40%
30%
20%
10%
0%
Siderophore uptake
Siderophore regulation
Unspecified Fe transport
Siderophore sysnthesis
Fe3+ uptake
Firmicutes
Cyanobacteria
Caldithrix
Bacteroidetes
Actinobacteria
β-Proteobacteria
α-Proteobacteria
Other δ-Proteobacteria
SAR324
Other γ-Proteobacteria
Methylococcaceae
SUP05
Alteromonadaceae

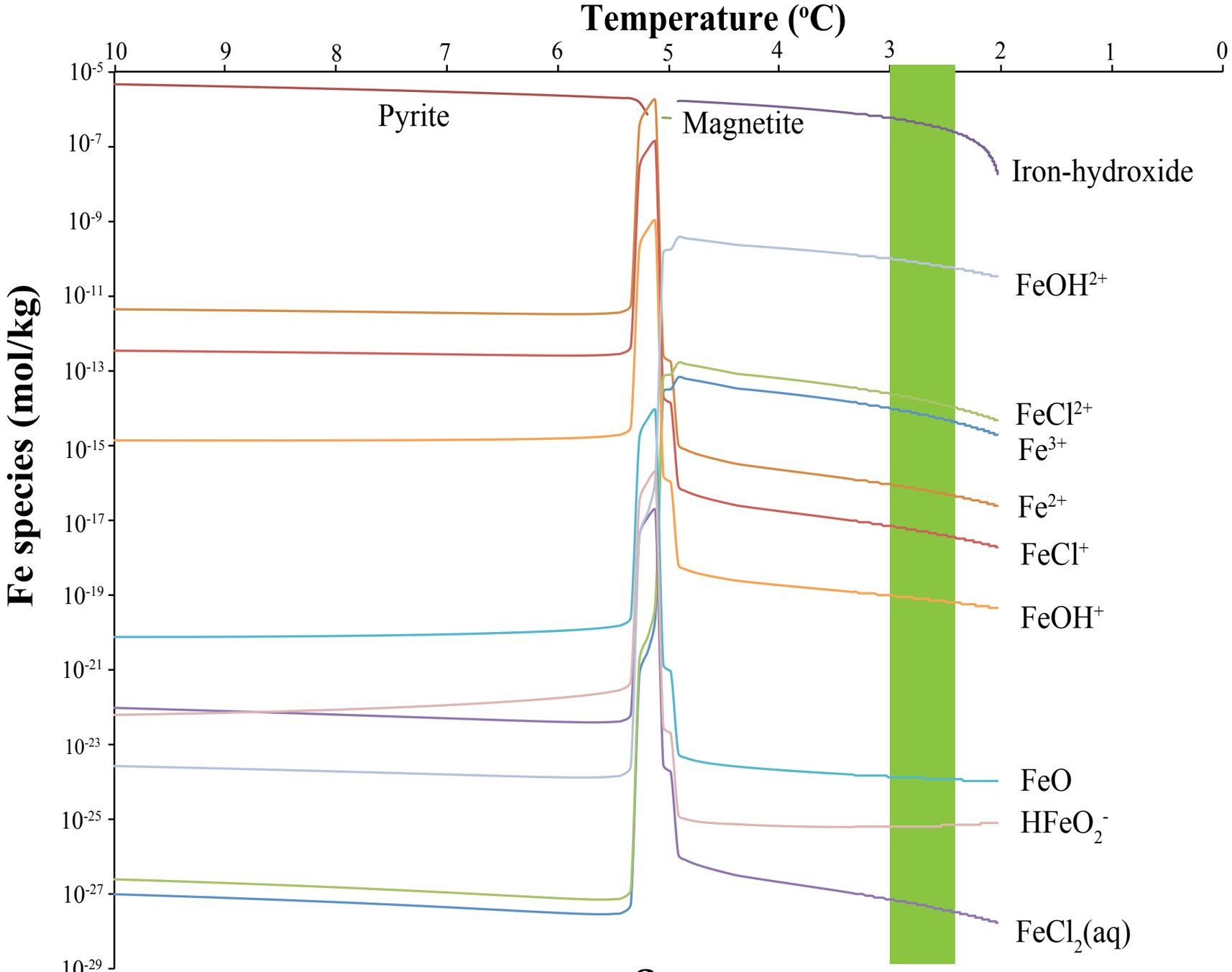
Temperature (°C)
10
9
8
7
6
5
4
3
2
1
0
Fe species (mol/kg)
10-5
10-7
10-9
10-11
10-13
10-15
10-17
10-19
10-21
10-23
10-25
10-27
10-29
Pyrite
Magnetite
Iron-hydroxide
FeOH2+
FeCl2+
Fe3+
Fe2+
FeCl+
FeOH+
FeO
HFeO2-
FeCl2(aq)

a

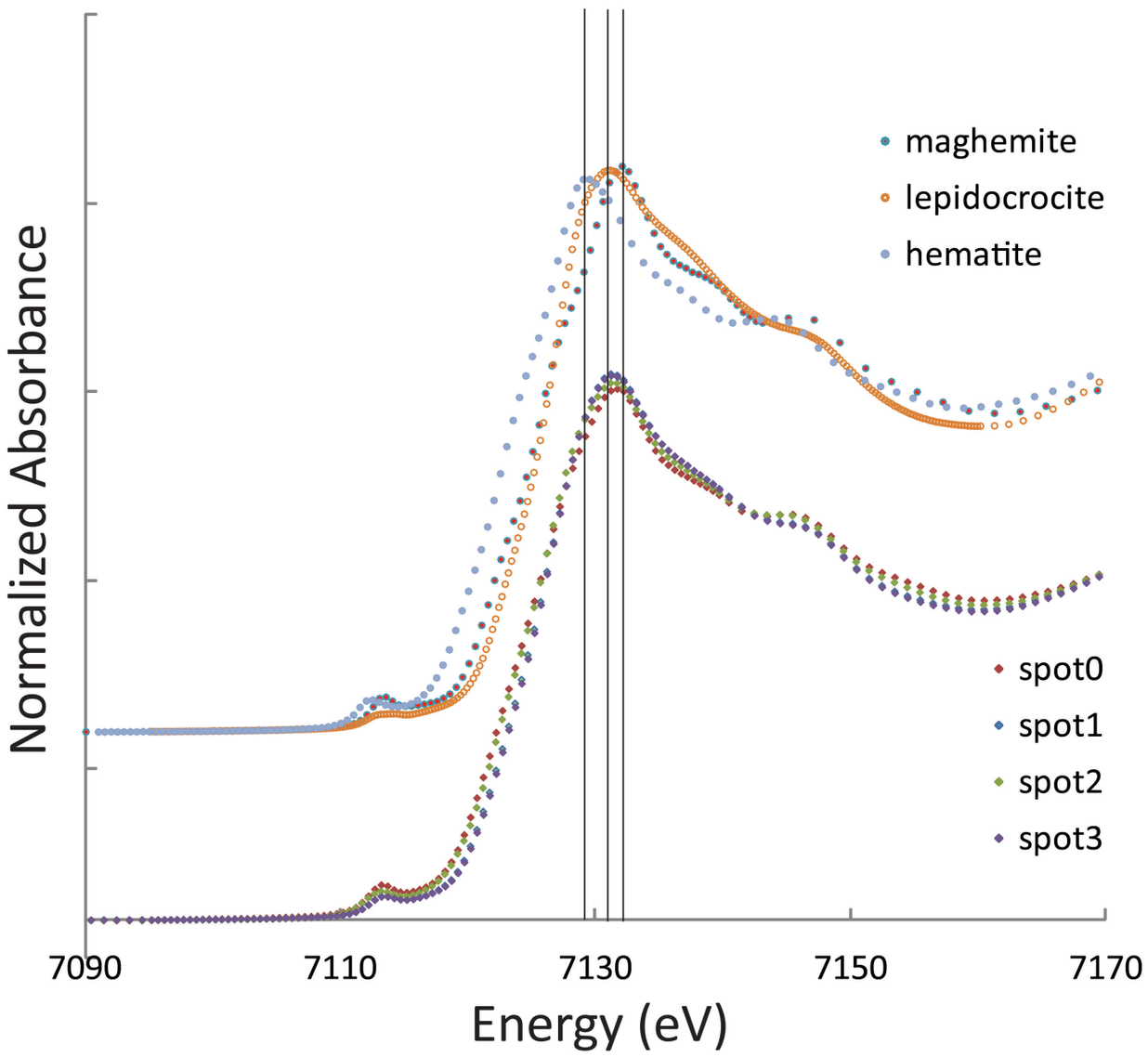
Normalized Absorbance
7090
7110
7130
7150
7170
Energy (eV)
maghemite
lepidocrocite
hematite
spot0
spot1
spot2
spot3

b

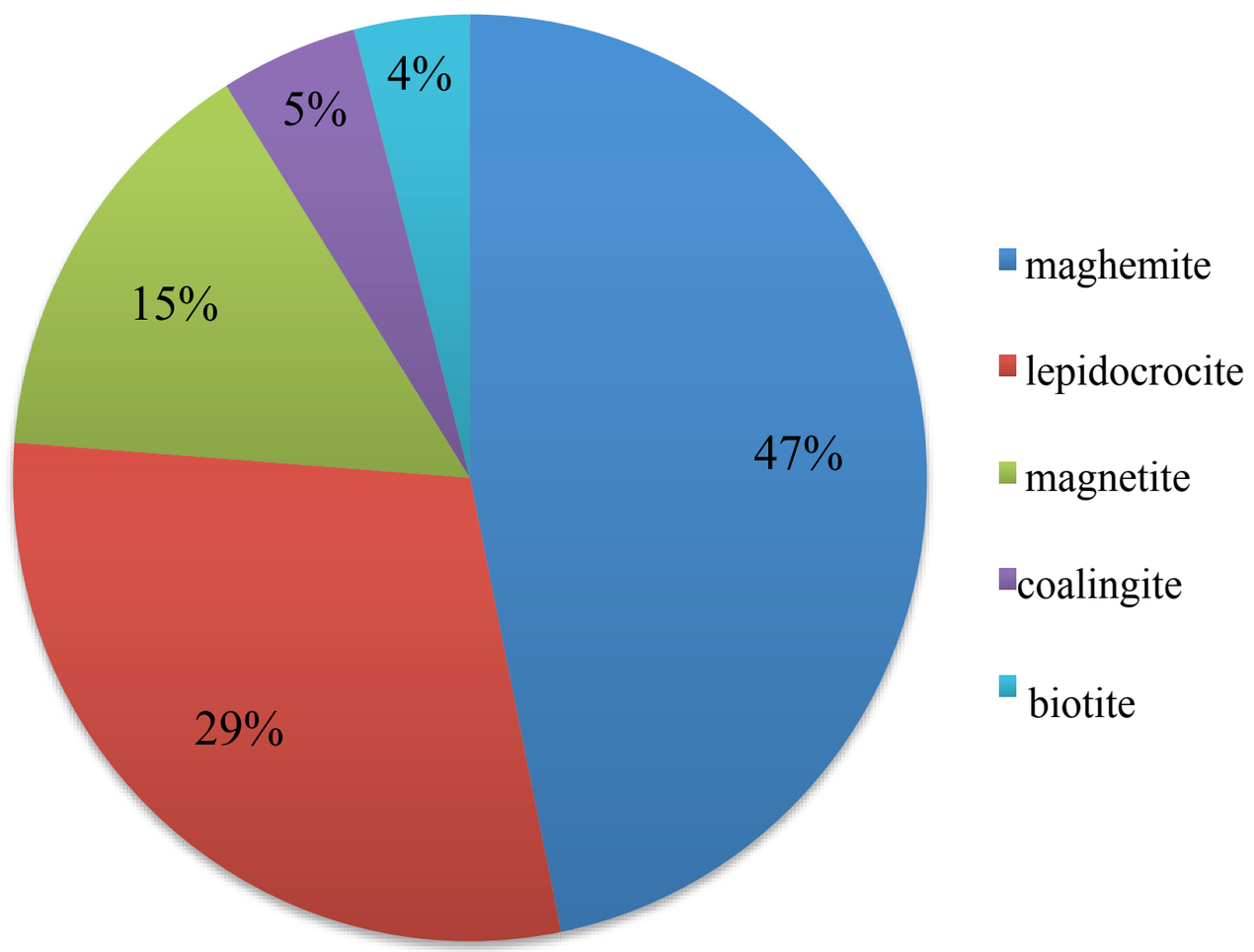
47%
29%
15%
5%
4%
maghemite
lepidocrocite
magnetite
coalingite
biotite

c

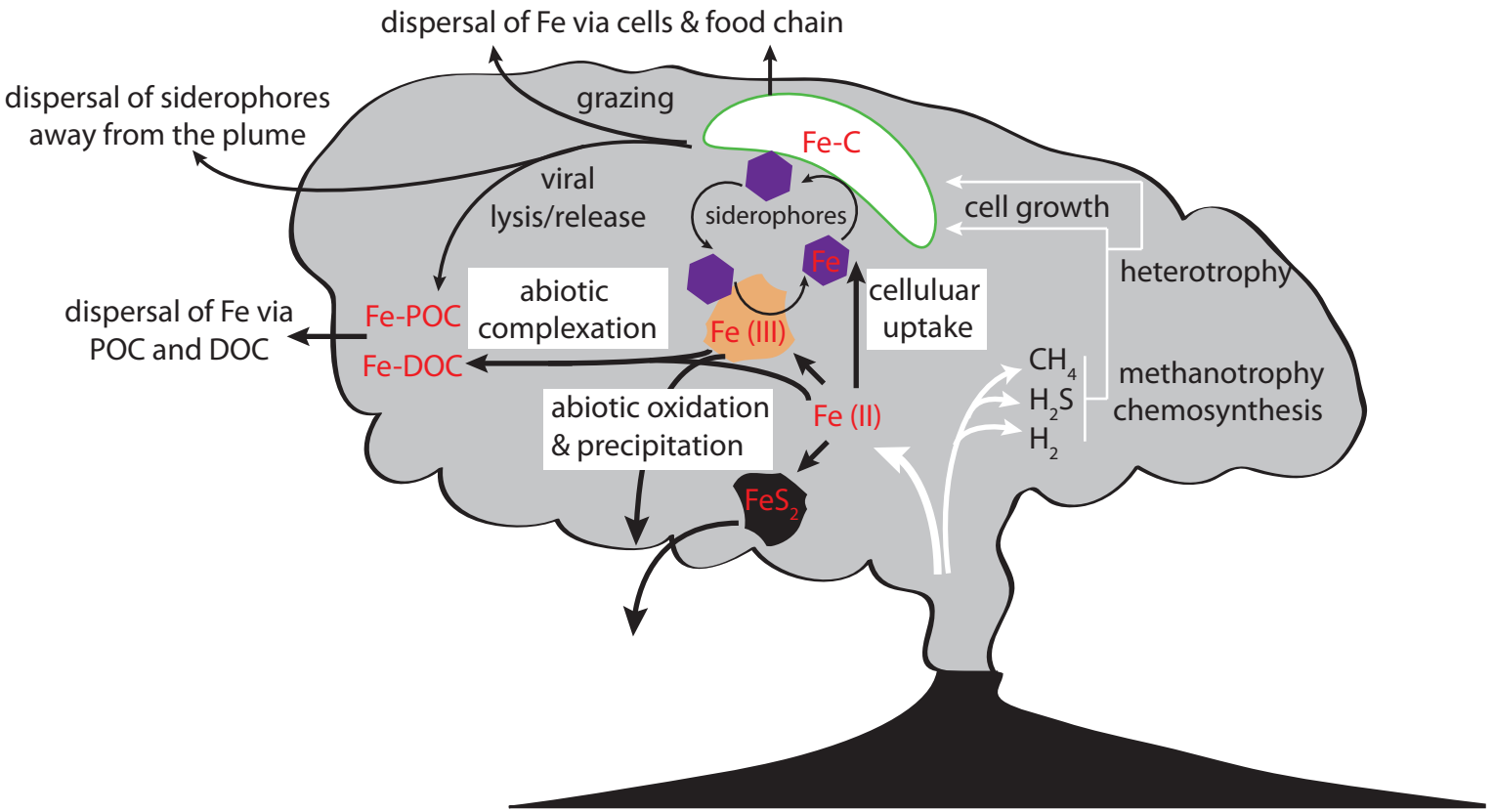
dispersal of Fe via cells & food chain
dispersal of siderophores away from the plume
grazing
Fe-C
viral lysis/release
siderophores
cell growth
heterotrophy
Fe
abiotic complexation
cellular uptake
dispersal of Fe via POC and DOC
Fe-POC
Fe (III)
Fe-DOC
CH4
H2S
H2
methanotrophy chemosynthesis
abiotic oxidation & precipitation
Fe (II)
FeS2